https://doi.org/10.5194/tc-2022-262
Preprint. Discussion started: 4 January 2023

The Cryosphere Discussions

Assimilating CryoSat-2 freeboard to improve Arctic sea ice thickness estimates

Imke Sievers[1,3], Till A. S. Rasmussen[1], and Lars Stenseng[2]

[1]Danish Meteorological Institut, Lyngbyvej 100, Copenhagen East, Denmark
[2]DTU Space, Danish Technical University, Elektrovej Bygning 328, 2800 Kongens Lyngby, Denmark
[3]Aalborg University, A. C. Meyers Vænge 15, 2450 Copenhagen, Denmark

Correspondence: Imke Sievers (imksie@dmi.dk)

Abstract. In this study, a new method to assimilate satellite radar altimetry derived freeboard instead of sea ice thickness is presented with the goal of improving the initial state of sea ice thickness predictions in the Arctic. In order to quantify the improvement in sea ice thickness gained by assimilating freeboard, we compare three different model runs. One reference run (refRun), one that assimilates only SIC (sicRun) and one that assimilates both SIC and FB (fbRun). It is shown that, estimates for both SIC and FB can be improved by assimilation, but only the fbRun improved the sea ice thickness estimates. The resulting sea ice thickness is evaluated by comparing it to AWI's weekly CryoSat-2 sea ice thickness data product, which is based on the same FB observations as were assimilated in this study. It is shown that, the sea ice thickness from the fbRun is closer to the traditional CryoSat-2 sea ice thickness than sea ice thickness from refRun or sicRun. Additionally, we compare independent sea ice draft measurements from the Beaufort Gyre Exploration Project to both fbRun sea ice thickness and observed CryoSat-2 sea ice thickness. This comparison shows that our new method provides equally good results as the AWI weekly CryoSat-2 product; in two of three locations even better results.

1 Introduction

With declining sea ice in the Arctic, marine traffic is increasing (Cao et al., 2022). This increases the demand for accurate sea ice predictions in order to ensure safety on the routes. Data assimilation is a commonly used tool to improve the initial state of sea ice predictions (Chen et al., 2017; Mu et al., 2018; Fiedler et al., 2022). In data assimilation, models and observations are combined using a number of approaches. For all approaches applies that, the variables that are assimilated need to be observable and need to affect the model variable that the assimilation aims to improve. Stroeve and Notz (2015) lists the sea ice volume and ocean heat content as the two model variables improving the models' sea ice forecast the most. Ocean heat content is difficult to observe on an Arctic-wide scale, but sea ice concentration (SIC) and sea ice thickness can be observed from satellites (Kwok, 2010; Laxon et al., 2013; Ivanova et al., 2014; OSISAF, 2017; Hendricks et al., 2021). While satellite observed SIC has a rather good accuracy and has been obtained since the late 1970s, satellite sea ice thickness observations have only been available since the early 2000s and come with large uncertainties (Laxon et al., 2003; Kwok, 2010). Several studies have found that sea ice thickness in contrast to SIC has a longer memory (Day et al., 2014; Stroeve and Notz, 2015;

https://doi.org/10.5194/tc-2022-262
Preprint. Discussion started: 4 January 2023

Dirkson et al., 2017) making it the more suitable variable to assimilate when aiming for an improved initial estimate of the Arctic sea ice.

The most commonly used data source for obtaining data to derive sea ice thickness from space is mounted on the ESA satellite CryoSat-2 (Drinkwater et al., 2004) orbiting the earth since 2010. Using an advanced radar altimeter, data from CryoSat-2 can be used to estimate the freeboard (FB) as the difference between the observed height of the snow/sea ice surface and the water level in leads between sea ice floes. To derive sea ice thickness from FB, a number of assumptions need to be made which will be discussed below. These assumptions lead to a large uncertainty of the resulting sea ice thickness estimate. This is why we are suggesting a method to directly assimilating FB instead of sea ice thickness.

Most of the existing sea ice thickness products use FB measurements to calculate sea ice thickness under the assumption of hydrostatic balance. The hydrostatic balance equation relates the sea ice thickness to FB, snow density, snow thickness, sea ice density and sea water density. In this relation, FB is measured and the other parameters are derived from climatology's or empirical values derived from in-situ observations (Ricker et al., 2014; Kwok and Cunningham, 2015; Tilling et al., 2018). The above mentioned uncertainties in satellite derived sea ice thickness originate to a large extent from the uncertainty of these parameters. Alexandrov et al. (2010) finds that, sea ice density introduces the largest error when calculating sea ice thickness from FB under the assumption of hydrostatic balance. Sea ice density depends on the ice age, where younger sea ice has a higher salinity due to more brine being enclosed in it. Over time brine is expelled into the ocean below. During the melt season, salt is washed out by melt water (Cox and Weeks, 1974), which makes multi year ice (MYI) less saline, and therefore less dense, compared to first year ice (FYI). Salt is not the only parameter responsible for variations in sea ice density. Enclosed gas is another parameter that makes sea ice density estimates uncertain. FYI sea ice density uncertainty is typically around 23.0 kg/m^3 and for MYI the uncertainty is around 35.7 kg/m^3 (Alexandrov et al., 2010). This high uncertainty originates from the difficulty of measuring sea ice density. The density varies within the ice column depending on whether the ice is below or above the sea level. On top of that, the harsh environment adds extra challenges in performing exact measurements (Timco and Frederking, 1996). Despite the variation of sea ice density, most products use fixed values of 917 kg/m^3 for FYI and 882 kg/m^3 for MYI (Sallila et al., 2019). The second biggest error contribution to sea ice thickness according to Alexandrov et al. (2010) is FB. Uncertainties in FB originate from uncertainties in the sea surface height, the location of the backscattering horizon and speckle noise (Ricker et al., 2014). Historically, snow thickness is derived from the Warren et al. (1999) snow climatology (W99), which is calculated from Russian drift stations during the period 1954–1991. Most of the included measurements were obtained on thick MYI. Kurtz and Farrell (2011) show that W99 is less reliable over FYI compared to MYI and Laxon et al. (2013) proposed a method to differentiate MYI and FYI snow thickness and snow density from W99. This method is today more commonly used in sea ice thickness products than the pure W99 climatology (Sallila et al., 2019). The uncertainty introduced by the snow thickness is heavily discussed (Kurtz and Farrell, 2011; Kwok et al., 2011; Laxon et al., 2013; Kern et al., 2015; Garnier et al., 2021). An alternative to W99 is to use a snow model to calculate the local snow thickness depending on precipitation. Fiedler et al. (2022) for example proves to have good results using snow thickness from the global coupled sea ice ocean model Forecast Ocean Assimilation Model (FOAM (Blockley et al., 2014)). W99 also includes a snow density climatology, which was commonly used in the calculation of sea ice thickness until 2020

https://doi.org/10.5194/tc-2022-262
Preprint. Discussion started: 4 January 2023

(Sallila et al., 2019). Mallett et al. (2020) found that approximating the snow density by a linear function improves the sea ice thickness estimate by about 10 cm. Resent sea ice thickness products, as for example Hendricks et al. (2021), have started to use the proposed seasonal linear approximation of snow density with good results. Sea water density only varies very little throughout the Arctic. Most CryoSat-2 sea ice thickness products use a single value of 1024 kg/m^3, which is the density at the freezing point of Arctic surface water. The influence of the uncertainty of this value on the hydrostatic balance equation is negligible (Kurtz et al., 2013).

The errors in sea ice density, FB, snow density, and sea water density add up when sea ice thickness is calculated from FB. Error estimates are used in data assimilation, for example in Kalman filters. Kalman filters build on knowing the model uncertainties, the observational uncertainties and the assumption that errors are unbiased and Gaussian distributed. Based on these assumptions the Kalman filter aim at deriving the best estimate. The better the error is known the better the resulting state estimate will be. CryoSat-2 derived sea ice thickness errors result not only from the above discussed errors, but also on how FYI and MYI areas are defined. The sea ice density, snow thickness and in some cases the snow density are calculated depending on the ice type. The ice type is derived from OSISAF ice type data, distinguishing between FYI, MYI and ambiguous ice type (Aaboe et al., 2021). In most CryoSat-2 sea ice thickness products, a small transitioning area is accounted for where a linear transitioning from MYI to FYI is assumed (Laxon et al., 2013; Tilling et al., 2018; Hendricks et al., 2021). The ice chart based sea ice type data product G10033 (Fetterer and Stewart, 2020) suggests large areas of mixed ice types. This area is significantly bigger and less homogeneous than the suggested area by the the linear transition between MYI and FYI based on OSISAF sea ice type. This means that sea ice density, snow thickness and snow density errors are systemically under/over estimated in this area of unambiguous ice type. Errors resulting from sea ice area estimates are not accounted for in most CryoSat-2 error estimates. The discussion above of the different origins of sea ice thickness error shows that estimating the uncertainty of sea ice thickness is complex. To avoid the use of a potentially biased sea ice thickness and an unreliable error estimate, this study suggests a method to assimilate FB instead of sea ice thickness. This is not to say that FB errors are unbiased. However, by choosing to assimilate FB, error contributions from snow thickness, snow density and sea ice density are eliminated. The challenge of this approach is that FB is not a sea ice model state variable but a diagnostic variable. A diagnostic variable is a variable not crucial to determine the model's physical state but it is calculated for output or minor parameterisations of processes within the model. Even though FB is not a state variable, it is related to sea ice thickness, which is a state variable, and can be calculated from FB under the assumption that a change in FB is only caused by sea ice thickness and modeled snow thickness, snow density and ice density are realistic.

In this study, we present an approach to assimilate FB directly into the sea ice model CICE (Hunke et al., 2017). In order to transform FB into the model state variable sea ice thickness, parametrisations and assumptions from the model and the forcing data are used. The method is implemented into CICE but should be applicable to any other model. This study mainly focuses on CryoSat-2 measurements but the approach presented could with small adjustments as well be applied to ICESat FB data (Martino et al., 2019). There are several studies mentioning approaches to assimilate FB (Vernieres et al., 2016; Kaminski et al., 2018; Fiedler et al., 2022), but to our knowledge this is the first paper presenting detailed descriptions on an assimilation method using FB instead of sea ice thickness.

https://doi.org/10.5194/tc-2022-262
Preprint. Discussion started: 4 January 2023

2 Methods and data

The following section presents all data sets, software and methods used to derive the sea ice thickness data sets evaluated in this study. The model is presented in section 2.1, the assimilation software PDAF is presented in section 2.2, the observational data is presented in section 2.3 and 2.4, and section 2.5 presents the observation data sets which are used for validation. The method for calculating the increment and how to convert it into sea ice model state variables is described in section 2.6. An increment is the amount of change of one assimilated variable after one assimilation time step.

2.1 Coupled ocean and sea ice model

The FB assimulation is implemented in a coupled sea ice (CICE v6.2, Hunke et al. (2021a)) and ocean model (Nemo v4.0, Madec et al. (2017)). The coupling is based on Smith et al. (2021), however both Nemo and CICE have been updated to more recent versions.

CICE is a multi-category sea ice model that consist of a dynamical solver, an advection scheme, and a thermodynamic column physics model called Icepack. CICE and Icepack are developed independently, but are by default linked. The model is run with 5 thickness categories with category bounds that follow a WMO standard setup. The upper bounds for the 5 categories (n) are: n=1: 0.3 m, n=2: 0.7 m, n=3: 1.2 m, n=4: 2 m, n=5: 999 m. In the presented study, CICE was implemented close to the default setup except that formdrag calculations, following Tsamados et al. (2014), were enabled.

The variables rho_i, rho_s, h_s and rho_w in section 2.6 are all defined in CICE or NEMO. The assimilation method for FB builds upon using model variables instead of empirical values. For this reason, we will describe how the used variables are calculated in CICE. The key variables are snow thickness, snow density and sea ice density. The snow thickness changes due to melt, precipitation, sublimation and flooding of ice when the sea-ice–snow interface lays below sea level. The snow thickness calculation follows a default CICE setup and was not changed for the assimilation. The CICE default snow density is uniform in time and space. We introduced a linearly varying snow density over the winter season to account for compression effects of the snow pack following Mallett et al. (2020). This density calculation is only used in the assimilation routine. In the rest of the model the density stays unchanged. The density of fresh ice is set to 882 kg/m^3 and the amount of brine is calculated. After this, the icepack function icepack_mushy_density_brine is used to calculate the brine density. Finally the density of fresh ice and brine is summed. The sea surface water density is calculated in NEMO.

The model domain is pan Arctic as shown by the red area in figure 1. NEMO is set up following (Hordoir et al., 2022). The lateral boundaries are located outside of the Arctic sea ice covered region such that sea ice boundary conditions are not required. The model is forced with 3 hourly ERA5 atmospheric forcing data, which consist of 2-m temperature, 2-m specific humidity, 10-m wind, incoming shortwave and longwave radiation, total precipitation, snowfall and air pressure at sea level (Hersbach et al., 2017). The lateral ocean boundaries are forced with monthly GLORYS12 data, which consist of salinity, temperature, u- and v-velocities (Lellouche et al., 2021). The ocean model includes tides and the tidal forcing at the open boundaries originates from the TPXO 7.2 harmonic tidal constituents (Egbert and Erofeeva, 2002) and river runoff is based on climatology from Dai and Trenberth (2002).

https://doi.org/10.5194/tc-2022-262
Preprint. Discussion started: 4 January 2023

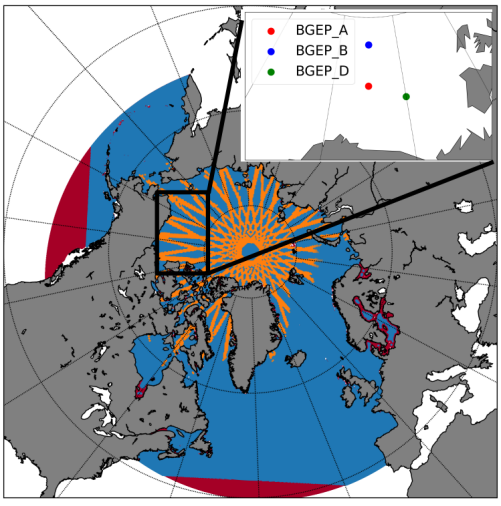

Figure 1. The red area indicates the model domain described in section 2.1, the blue area shows the OSISAF SIC data coverage and the orange lines give an example coverage of one week of CryoSat-2 data. The zoomed area shows the location of the three moorings described in section 2.5.

All model output discussed in the following sections is calculated based on daily means.

2.2 PDAF

No measurement nor model is perfect, as both have biases and uncertainties. If the errors are known and independent, a Kalman filter can be used to calculate the best estimate of the variable in question. The Parallel Data Assimilation Framework (PDAF), which is developed by the Alfred Wegener Institute for Polar and Marine Research (AWI), provides portable ensemble Kalman filters and other assimilation routines. In this study the parallelized offline version of the Local Error Subspace Transform Kalman Filter (LESTKF) (Nerger et al., 2012) was implemented. The LESTKF has prior to this study successfully been used to assimilate SIC and sea ice thickness by for example Chen et al. (2017). The optimal SIC and FB state estimate resulting from the LESTKF is calculated based on the model uncertainty and observational errors. In this study we set the observational errors for SIC to 15 % and the FB error to 0.15 m and the model uncertainty is calculated from the ensemble variance. For the simulations described here, a static ensemble was created from a initial model run, which ran from 1995-2020 without assimilation. From analysing this run it is known that the model has biases in SIC and FB. To account for these biases, the variance was increased by including model states from month ahead and prior to the assimilation time. To create the static ensemble, the years 2010-2020 were used.

The ensemble is calculated from the initial model run by calculating the mean model state from 80 days of the initial run and subtracting it from each of the 80 model states. The resulting variations where added to the current model state of the assimilation model run. The variance of the resulting 80 ensemble members was used to calculate the model uncertainty within PDAF. As mentioned above, to correct for model biases only 72 days of the ensemble members were chosen $\pm$ four days

https://doi.org/10.5194/tc-2022-262
Preprint. Discussion started: 4 January 2023

around the assimilation time step. This means that, eight model states per year were chosen closest to the current assimilation day from the ten year time period of the initial run. Taking an assimilation on 01-11-2020 as in example, this means that for the year 2010-2019 the days 28-10-20?? to 04-11-20?? are chosen. In the last year eight ensemble members were taken from $\pm$ three month from the assimilation time step, as described in figure 2. If dates lay outside the initial runs time frame, dates from the beginning of the initial run were chosen. Again taking an assimilation on 01-11-2020 as in example, this means that last eight days chosen are 28-07-2020 to 31-07-2020 and 01-02-2010 to 04-02-2010. The increment inc refereed to in section 2.6 is calculated by subtracting the PDAF analysis state from the model ensemble mean. The resulting increment is negative if SIC or FB should be increased in the current model grid location, positive if the variable should be decreased and zero if no assimilation is performed. In the end of each assimilation step, PDAF was run twice, once to calculate the SIC increment and once to calculate the FB increment. The localisation radius used equals 60 grid cells and the localisation is weighted with a 5th-order polynomial function.

2.3 CryoSat-2 radar altimetry freeboard

The observed FB assimilated in this study is level 3 weekly gridded CryoSat-2 radar FB downloaded from the Alfred Wegener Institutes (AWI) sea ice portal (version 2.4 (Hendricks et al., 2021)). It is gridded, along track data on the EASE2-Grid with a 25 km resolution. The radar FB is defined as the elevation of retracked point above instantaneous sea surface height without snow range correction. The data product is derived from the CryoSat-2 baseline E data, the DTU21 mean sea surface model, and the "Threshold First Maximum Retracker Algorithm" (TFMRA) (Ricker et al., 2014).

With the onset of melt in the beginning of summer, melt ponds are formed on the sea ice surface. The radar signature from melt ponds is comparable to the signature from leads, which can result in ambiguous determination of the sea surface height by including melt ponds observations as lead observations. This ambiguity results in a larger bias in the FB measurements, and FB data is therefore only assimilated from November to March, where we do not expect melt ponds. The uncertainty of the radar FB given in the AWI data set ranges from approximately 0 - 0.07 m in the chosen month. The data set was interpolated to the model grid with help of CDO (Schulzweida, 2022). An example of the FB data assimilated per one assimilation time is indicated by the orange area in figure 1.

2.4 OSISAF data

Ocean and Sea Ice Satellite Application Facility (OSISAF) SIC is assimilated in this study. It is based on the Special Sensor Microwave Imager / Sounder (SSMIS) passive microwave measurements, which is a polar orbiting satellite that hosts a linear polarised passive microwave radiometer. The OSISAF algorithm combines SSMIS microwave measurements with numerical weather prediction (NWP) model output from ECMWF in order to calculate SIC. Passive microwave measurements are independent from visible light, which makes this sensor type especially suitable in polar regions. The data used is level 4 and it is gridded on a 10x10 km grid once a day and has a accuracy of $\pm 10\%$ (OSISAF, 2017).

For the assimilation the data set was interpolated on to the model grid using CDO (Schulzweida, 2022). The resulting SIC data coverage assimilated is indicated by the blue area in figure 1.

https://doi.org/10.5194/tc-2022-262
Preprint. Discussion started: 4 January 2023

2.5 Validation data

The sea ice thickness output from the assimilation is compared to two different sea ice thickness data sets. The first data set is based on the same data set which is included in the AWI CryoSat-2 FB, which is described in section 2.3. This data set also includes an estimate of the ice thickness. In order to obtain sea ice thickness from FB hydrostatic balance is assumed and sea ice thickness is calculated as described in equation 4. In the AWI CryoSat-2 data set, the snow thickness from Warren et al. (1999) snow climatology was applied over MYI and NSIDCs AMSR2 snow depth was applied over FYI. The snow density is treated following Mallett et al. (2020) and the sea ice density is set to 916.7 kg/m^3 for FYI and to 882.0 kg/m^3 for MYI and FYI is distinguished with the help of OSISAF ice type data. For a more detailed description of the data set see Hendricks et al. (2021).

The ice thickness data set is based on the same FB data as was assimilated, but it uses different constants when compared to the sea ice model. For these reasons it can not be viewed as completely independent from the sea ice thickness derived based on the FB assimilation routine. In order to compare to an independent sea ice thickness data set, the Beaufort Gyre Exploration Project (BGEP) upward looking sonar (ULS) data is used to validate against stationary point measurements. It can be downloaded from www2.whoi.edu. The upward looking sonar data is obtained from three locations named mooring A, B and D, marked with red, green and blue dots in figure 1. The instruments are located 50-85 m below the water surface and measure the ice draft every 2 s over a 2x2 m area. The signal is filtered and averaged over 10 second intervals in order to correct for tilting errors. The sea ice draft accuracy is ± 5 cm. In this study, the full resolution 10 second data set was used. The daily average and standard derivation was calculated from the differences of all 10 second measurements and the model daily output. The model and AWI draft was calculated as sea ice thickness minus sea ice FB. The advantage of the BGEP data is that it is completely independent of the assimilated data, however the upward looking sonars only cover a small area of the Arctic.

2.6 Assimilation routine

Three parallel simulations are carried out in order to demonstrate the assimilation framework. Each run is 3 years, if assimilation is applied it is applied on a weekly basis. The reference run (RefRun) includes no assimilation. The SIC assimilation run (sicRun) includes only SIC assimilation from November to March, and the full assimilation run (fbRun) includes both SIC and FB assimilation from November to end March. The workflow in figure 2 applies to the weeks with assimilation only. During the period April to October no assimilation is performed.

In the following text we distinguish between the model time step (600 sec) and the assimilation time step (one week). In the first assimilation time step (2018-01-01), the model is initialized from restart files containing the state variables from CICE and NEMO from an initial model run without assimilation from 01-01-1995 to 31-12-2017. The output from this run is also the input for PDAF together with the FB or SIC observations from the same time period (shown in figure 2). PDAF calculates the best state estimate for FB and/or SIC as described in section 2.2. The difference between the resulting analysis state and the model state is called the increment. The increment is negative where the model state needs to be increased and positive where the model state needs to be decreased in order to match the best state estimate calculated by PDAF. The assimilation

https://doi.org/10.5194/tc-2022-262
Preprint. Discussion started: 4 January 2023

described in the following is only performed where the increment is !=0. The increment is read in CICE just after the model was initialized from restart files, and the increments are spread linearly over the assimilation time step, to avoid discontinuities, following equation 5. Until this step both SIC and FB are treated equally. SIC is a model state variable, while FB needs to be converted into a model state variable before it's increment can be subtracted from the model.

2.6.1 SIC assimilation

The SIC increment is divided by the number of time steps (number of model time steps in one assimilation time step), which results in the fractal increment or the amount of SIC change needed per model time step (following equation 5). This fractal increment is here after subtracted at each time step from the model value. The model used in this study is a multi category model. Therefore the grid cell average increment must be spread over the five model categories. To achieve this equation 1 was used. Here var_{old} is the SIC from the restart file, $var_{old}(n)$ is the SIC in the n categories, inc_{icon} is the SIC increment and n is the thickness category.

$$var(n) = var_{old}(n) - var_{old}(n)\frac{inc_{var}}{var_{old}} \tag{1}$$

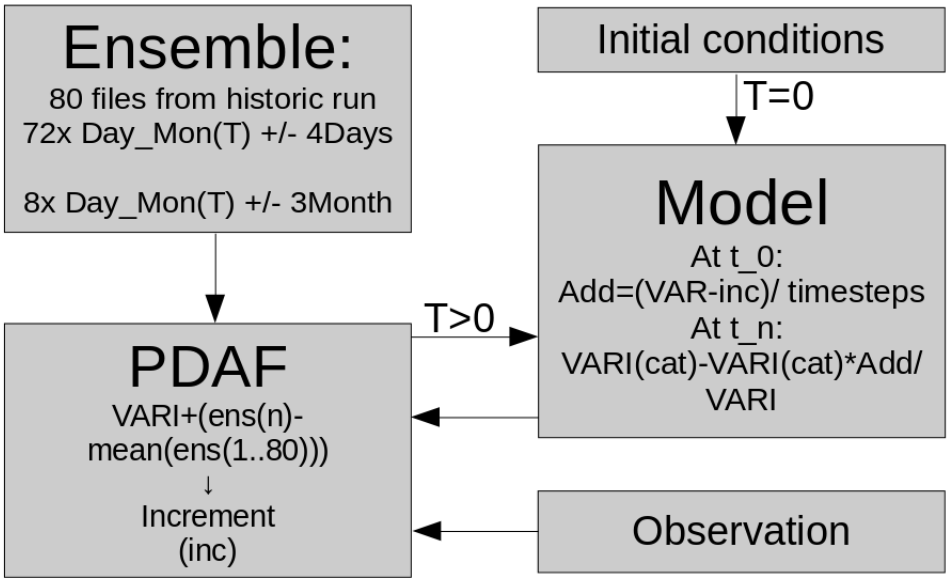

Figure 2. Data flow chart of the full assimilation set up including calculations relevant for the assimilation. Arrows indicate data exchange. Time steps indicated with a T are assimilation time steps and time steps indicated with a t are model time steps.

If no sea ice exist where the increment is !=0 prior to the assimilation, 10 cm ice is added in the thinnest category, and 2 cm snow is added on top.

https://doi.org/10.5194/tc-2022-262
Preprint. Discussion started: 4 January 2023

2.6.2 FB assimilation

After the SIC increment is added a check is performed deciding whether or not to assimilate FB. FB measurements are less reliable in areas where large areas of open water are present due to the stronger radar backscatter from the water surface in comparison to the ice surface. Therefore, FB assimilation is done if SIC is larger than 80 % and if the sea ice thickness is above 0.05 cm.

Since FB is not a model state variable, it needs to be transformed into sea ice thickness before it can be treated similar to the SIC increment in equation 1. As a first step, the model radar FB is calculated from the model sea ice and snow variables at restart time following equation 2. Here hi is the model sea ice thickness, rho_w sea surface water density, rho_i sea ice density, rho_s snow density and h_s snow thickness. All variables are set in CICE. $corr$ is a correction term following equation 3 following Mallett et al. (2020). After the FB increment at model time step 1 is read in it is added to the model radar FB.

$$FBr_0 = \frac{hi(rho_w - rho_i) - rho_s h_s}{rho_w} - corr \tag{2}$$

The variables rho_i, rho_s, h_s and rho_w are variables used in equation 2, 3 and 4 and are CICE model variables. For a more detailed description on how they are calculated see section 2.1. Mallett et al. (2020) found that representing the seasonality of snow density in by a linear function improves the sea ice estimate by up to 15 cm. The study refers to an improvement based on equation 3. The correction term is described in equation 3, where c is the speed of light in vacuum and cs the speed of light in snow. For consistency we use the same snow density through out all calculations.

$$corr = (h_s(\frac{c}{cs} - 1.) \tag{3}$$

After the model radar FB (FBr_0) was calculated following equation 2, the increment (FB_{inc}) was read in at t_0. FB_{new} for equation 4 is calculated following $FB_{new} = FBr_0 - FB_{inc}$. FB_{new} is the FB that is the best FB estimate according to the PDAF analysis and is only calculated at t_0.

$$new_{ice} = \frac{rho_s h_s + rho_w(FB_{new} + corr)}{rho_w - rho_i} \tag{4}$$

Still at t_0, the sea ice thickness from equation 4 is then subtracted from the modeled sea ice thickness initialized from the restart files and divided by the restart time step ($time_r$) as shown in equation 5.

$$inc = \frac{var_0 - new_{ice}}{time_r} \tag{5}$$

Equation 5 results in the sea ice thickness increment, which is added at each assimilation time step following equation 1 to be distributed over the n categories. In equation 5 var_0 is the variable being assimilated (SIC or sea ice thickness), the term $var_0 - new_{ice}$ is the increment read in at t_0 (when SIC is assimilated), or calculated from equation 4 (when FB is assimilated) and $time_r$ the amount of time steps over which the increment is spread. After the sea ice thickness increment, to be applied at each time step, was calculated following equation 5, the sea ice thickness increment is added in all categories following equation 1. After each assimilation, the CICE function cleanup_itd is run to ensure that the sea ice thickness in all categories lies within the set range as defined in 2.1.

https://doi.org/10.5194/tc-2022-262
Preprint. Discussion started: 4 January 2023

3 Results

3.1 Freeboard and Sea Ice Consentration RMSE

In order to verify that the assimilation improves modeled FB and SIC, the RMSEs between the assimilated data sets and the model variables were computed after each assimilation time step. The calculation of RMSE includes all data points that serve as PDAF input. This means that, the RMSE for FB was calculated inbetween the area marked orange in figure 1 and the corresponding model values. Equally for SIC, the blue area in figure 1 and the corresponding model data were used. The results are shown in figure 3 and 4 upper panel, and they are calculated from mean weekly model output data at the location where the corresponding observation was assimilated on a weekly bases. The lower panels in figure 3 and 4 show the difference between refRun and sicRun and refRun and fbRun that express the amount of change caused by the assimilation. Positive values indicate that the assimilation has improved the SIC or FB, and negative values indicate that the variable was degraded by the assimilation.

Figure 3 upper panel shows that the refRun (red) has the highest RMSE over all and increases the most over the assimilation period. The sicRun (green) and fbRun (blue) RMSE increase over the assimilation period, but to a lower degree than the refRun. This is also shown by figure 3 lower panel, which shows a steady increases in the difference between refRun and the assimilated runs (sicRun and fbRun). There are negative values in the lower panel in October for the last two of years, which indicates that the assimilated runs agree less with the assimilated data than the refRun in the beginning of the assimilation period. The RMSE difference in figure 3 lower panel falls below 0 in the beginning of all assimilation periods after the initial one. Figure 4 shows the RMSE of all FB values assimilated at the corresponding time in the upper panel. The FB RMSE for the refRun (red) and the sicRun (green) are almost equal throughout the assimilation period. Both RMSEs range between 7 cm and 14 cm. The FB RMSE for fbRun shows a clear drop with in the first month of the assimilation period to about 5 to 6 cm. The RMSE differences in figure 4 lower panel are all above 0, even in the beginning of a new assimilation period in November. It is expected that the SIC RMSE in figure 3 and the FB RMSE in figure 4 show improvements as the observation values are used within the assimilation scheme.

3.2 CryoSat-2 AWI sea ice thickness

In order to show that the sea ice thickness from the FB assimilation method gives comparable good sea ice thickness estimates as other CryoSat-2 derived sea ice thickness products the fbRun sea ice thickness was compared to the AWI sea ice thickness. The AWI sea ice thickness was chosen since it is derived from the same FB values as the FB assimilated in fbRun. Therefore differences can illustrate the impact of changing the method of converting FB to ice thickness.

The regression density plots in figure 5 show the correlation between the AWI sea ice thickness and the fbRun sea ice thickness in orange and the correlation between the AWI sea ice thickness and the refRun sea ice thickness in blue. The left plot shows the data at the beginning of October 2019 and the right plot at the end of the winter 2019/2020 (March 2020). In October both model runs have a clear thin bias compared to the AWI sea ice thickness data set. This is more pronounced in the refRun compared to the fbRun. In October the maximum sea ice thickness of the refRun is approximately 1.5 m whereas the

https://doi.org/10.5194/tc-2022-262
Preprint. Discussion started: 4 January 2023

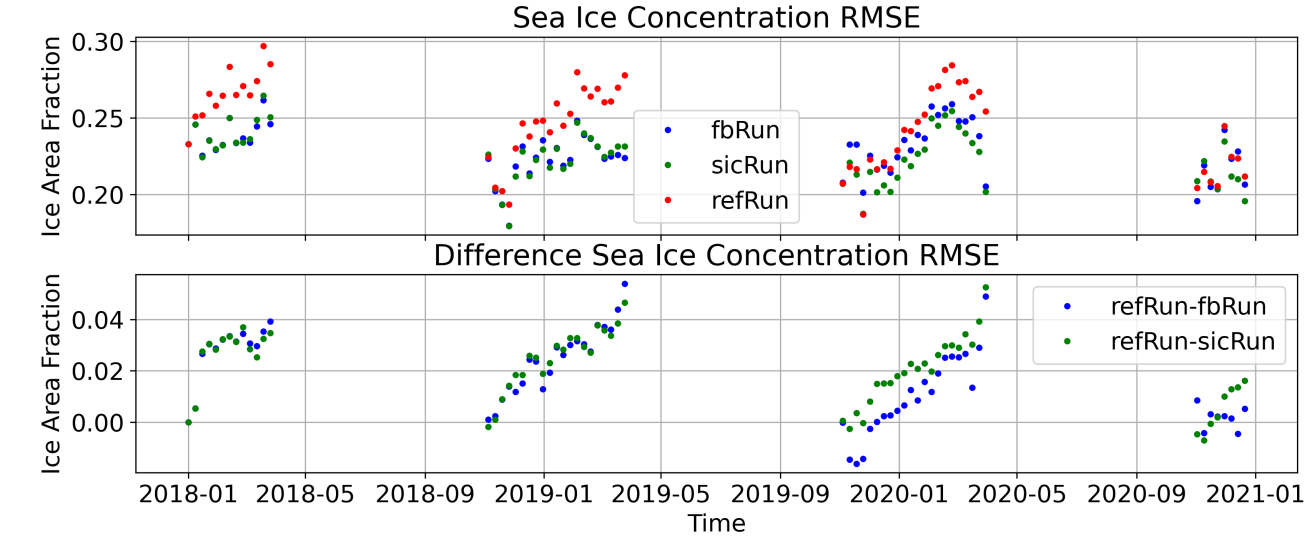

Figure 3. Top panel: Weekly SIC RMSE calculated at the observation data location averaged over the corresponding assimilation time step. The blue dots show the fbRun RMSE, the red the refRun and the green the sicRun. Lower panel: The difference of the top panel RMSE of refRun-fbRun in blue and refRun-sicRun in green.

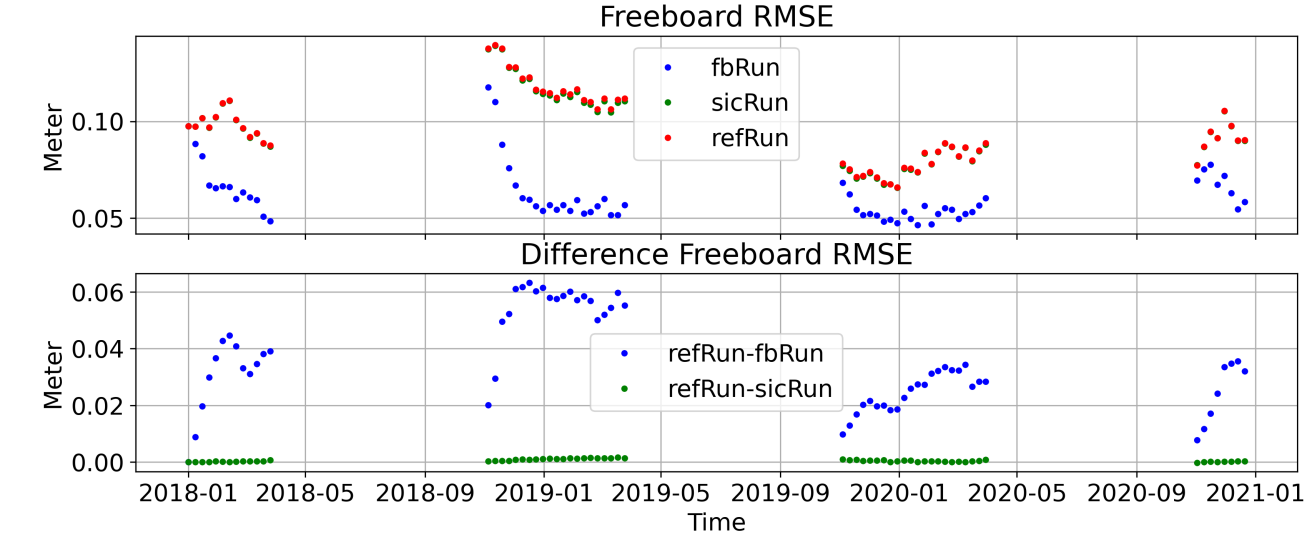

Figure 4. Top panel: Weekly FB RMSE calculated at the observation data location averaged over the corresponding assimilation time step. The blue dots show the fbRun RMSE, the red the refRun and the green the sicRun. Lower panel: The difference of the top panel RMSE of refRun-fbRun in blue and refRun-sicRun in green.

https://doi.org/10.5194/tc-2022-262
Preprint. Discussion started: 4 January 2023

maximum sea ice thickness of the fbRun is approximately 1.9 m. The maximum AWI sea ice thickness is approximately 2.9 m. The most dominant sea ice thickness in the AWI sea ice thickness data set is around 1.5 m and both the fbRun and refRun dominant sea ice thickness is around 0.8 m. In March the maximum sea ice thickness for the fbRun is around 3.2 m and for the refRun it is around 2.9 m, whereas the maximum of the AWI sea ice thickness product is around 4 m. The dominant sea ice thickness in the AWI product lies around 1.8 m, for the fbRun around 1.1 m and for the refRun around 1.8 m. Even though the maximum of the AWI sea ice thickness and the sicRun sea ice thickness agree better, overall are the sea ice thicknesses from the refRun and the AWI sea ice thickness in better agreement. In March, both the fbRun and the refRun have more grid cells with thin ice compared to the AWI data set and less with thick ice. This is more pronounced in the refRun. The AWI sea ice thickness is overall thicker.

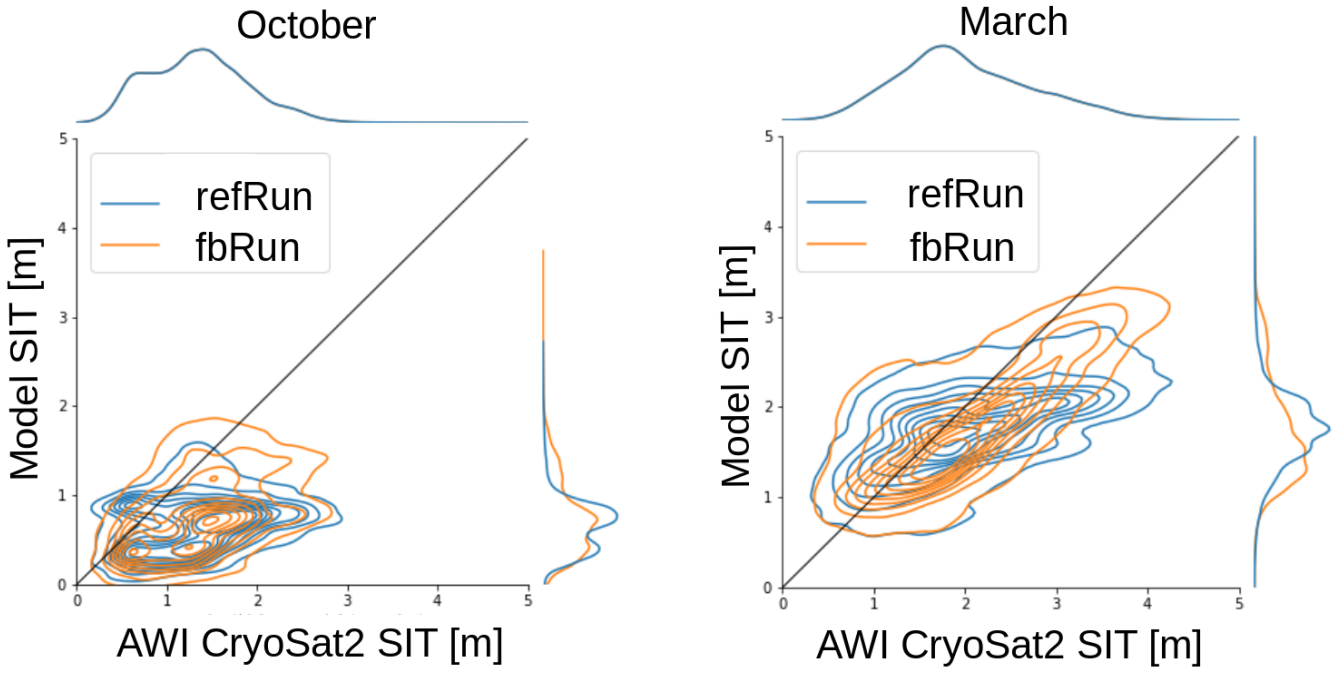

Figure 5. Regression density plot of assimilated sea ice thickness at initially observed radar FB locations and AWI sea ice thickness data product, derived from same FB observations. The right panel shows the data for the last week of March and the left panel the data for the last week of October. The blue lines show regression density between the data product on the x axis and the refRun sea ice thickness on the y-axis and the orange lines the observations in relation to fbRun sea ice thickness. The black line shows an ideal linear regression.

Figure 6 shows the differences between the AWI CryoSat data product, the refRun and the fbRun on the 03-30-2020, which is the last assimilation time step in the third assimilation season. From left to right the figure shows the difference between AWI sea ice thickness and refRun sea ice thickness, AWI sea ice thickness and fbRun sea ice thickness, AWI snow thickness, used to derive the AWI sea ice thickness, and the fbRun snow thickness and the sea ice density used to derive the AWI sea ice thickness and the sea ice density from the fbRun. The first two panels from left show that the fbRun sea ice thickness is closer to the AWI

https://doi.org/10.5194/tc-2022-262
Preprint. Discussion started: 4 January 2023

sea ice thickness in most places except in the Beaufort Sea where the sea ice thickness was in good agreement between the AWI data and the refRun in comparison to the fbRun. The largest differences between the AWI sea ice thickness and the refRun is located in the central Arctic and north of Canada and Greenland ranging from 1-1.5 m. For the fbRun the largest differences is around 1-1.5 m, which is found off the Canadian archipelago and in the eastern Beaufort Sea. This area of maximum sea ice thickness difference is significatly smaller than the area of >1 m differences in figure 6 A). In the central Arctic, the difference between the AWI sea ice thickness and fbRun sea ice thickness is around 0.5-0.8 m. The largest differences in snow thickness are located in the Barents Sea and Kara Sea (figure 6 C)). The largest differences in sea ice density are located around the Beaufort sea and the eastern Arctic Ocean (figure 6 D)). The snow thickness differences and sea ice density differences show a clear pattern related to the areas of FYI and MYI used to determine the sea ice density and snow thickness in the AWI data set. The same pattern is not shown in the sea ice thickness differences.

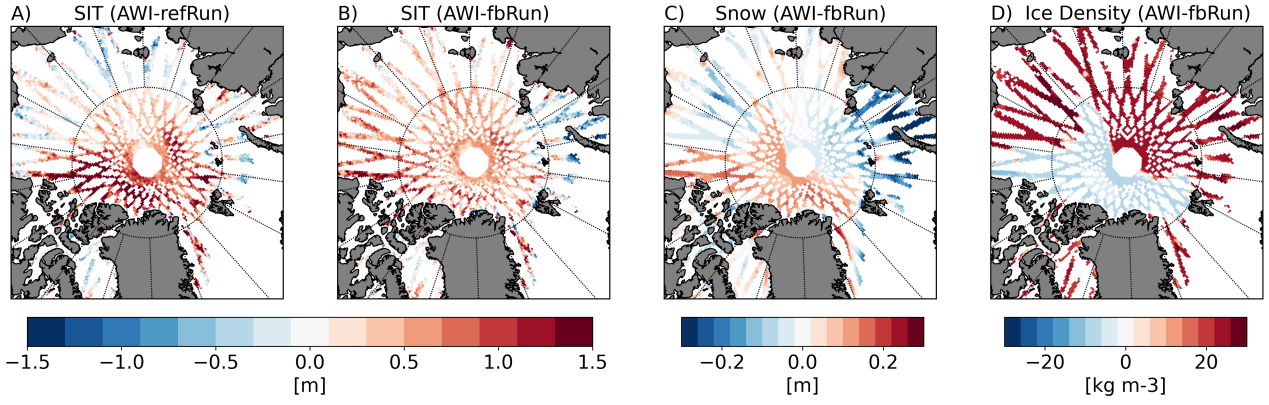

Figure 6. Shows the differences between the AWI sea ice thickness product and the model values at 2020-03-30 for: a) the AWI sea ice thickness minus the sea ice thickness from the refRun, b) the AWI sea ice thickness minus fbRun sea ice thickness, c) the difference between the AWI data set snow thickness and the fbRun snow thickness and d) the difference between the sea ice density from the AWI data set minus the fbRun sea ice density.

3.3 Upward looking sonar data

The BGEP upward looking sonar sea ice draft is independent of the observed FB data, and it is used for the comparison of the modelled sea ice draft, which is calculated as described in section 2.5. The BGEP data is not available for the complete period from 01-01-2018 to 31-12-2020, hence only data from October 2018 to December 2020 is used.

The daily mean differences between BGEP upward looking sonar ice draft and model ice draft are shown in figure 7. The observation data has a frequency of 10 seconds, whereas the frequency of the model data is daily. To derive the mean and standard derivation (std) of the difference between observations and model only observations from the same day as the model date were used. Only the model grid point nearest to the observation location was used for this calculation. Figure 7 shows the daily mean differences with corresponding standard derivation for a 7 days rolling mean from the mooring locations shown in

https://doi.org/10.5194/tc-2022-262
Preprint. Discussion started: 4 January 2023

figure 1. The dashed line shows the fbRun, the solid line the refRun, and the dotted dashed line the sicRun. The gray shaded areas indicate the assimilation period.

For all three moorings, fbRun shows the values in closest agreement with the observations throughout the entire period displayed. The refRun and the sicRun are almost in perfect agreement except for a few time steps as for example in October 2019 at BGEP mooring A and D. The mean differences between fbRun and observation is -0.18 m with a mean standard derivation of 0.67 m. The mean difference between the refRun and the observation is -0.57 m and the mean standard deviation is 0.67 m. Periods in summer, when the observation std is 0 m, indicates periods with no ice present. Gaps indicate periods where no data is available. The BGEP observations are all ice free in summer 2019 while only fbRun at BGEP mooring A reaches the point of being ice free in late September until beginning of November 2019.

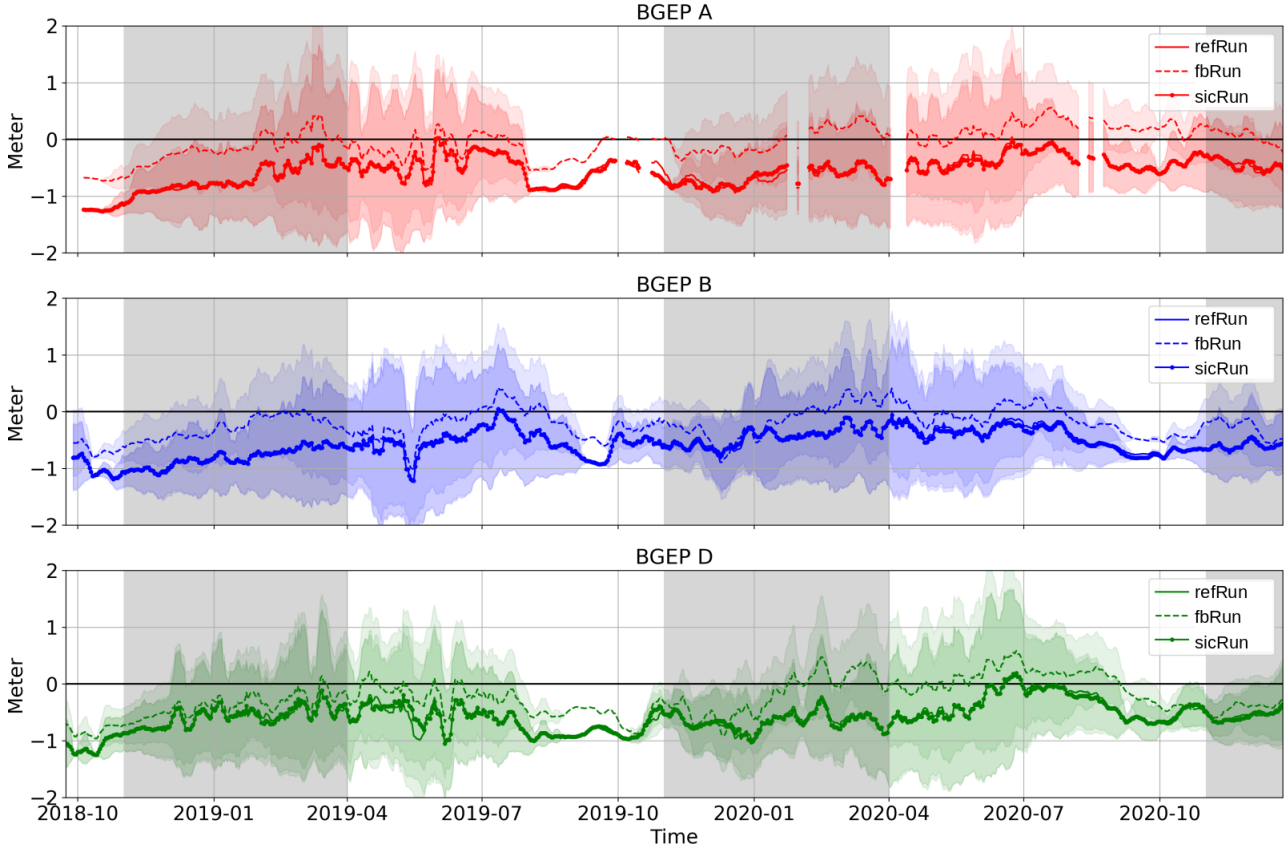

Figure 7. Daily mean sea ice draft observation — model differences. The 10 seconds data record from the moorings were averaged and the model values subtracted from them. The shaded colored background shows one standard derivation calculated for each day from the 10 seconds record. The gray shaded area indicates the assimilation period. The dashed line shows observed sea ice draft minus fbRun sea ice draft, the solid line the refRun and the dot-dashed line the sicRun only. The upper panel shows data from mooring A, the middle panel data from mooring B and the lower one from mooring D. The sites are marked in the corresponding colors in fig 1.

https://doi.org/10.5194/tc-2022-262
Preprint. Discussion started: 4 January 2023

Table 1. The mean RMSE of the weekly mean differences shown in figure 8. The RMSE was calculated on average for each mooring and both the fbRun ice draft and the AWI CryoSat-2 ice draft. All values are given in meters.

	BGEP mooring A	BGEP mooring B	BGEP mooring D
fbRun	0.193 m	0.307 m	0.381 m
AWI CryoSat-2	0.220 m	0.324 m	0.377 m

In the Beaufort Sea, where the BGEP moorings are located as shown in figure 1, the differences between fbRun and the AWI sea ice thickness (second left panel in figure 6) is significant. Since the the AWI sea ice thickness is not an in-sito observation, but the BGEP moorings are, all three data sets were compared in figure 8. Figure 8 shows the mean differences between the AWI sea ice draft and the fbRun sea ice draft. To do so, the AWI data set was interpolated to the model grid and only data points covered by all three data sets (AWI CryoSat-2, fbRun and BGEP) were considered. Instead of daily averages as shown in figure 7, weekly averages were calculated since the AWI sea ice thickness comes in weekly time steps. The "+" in figure 8 show the AWI data, and the diamonds the fbRun data. The gray background shows the assimilation period. Colors are chosen per mooring according to figure 1. The resulting differences between the fbRun and the AWI CryoSat-2 sea ice draft are shown in figure 8. Both the AWI sea ice draft and the fbRun sea ice draft differ about $\pm$ 50-70 cm from the mooring data. There is no clear bias, or seasonality in either differences and they don't always follow the same pattern, except in winter 2019/2020 where both data sets begin with a negative bias and end with a positive bias, with the exception of a few weeks in the AWI CryoSat-2 draft in the end of the assimilation period.

The RMSEs between the BGEP moorings sea ice draft, the fbRun sea ice draft and AWI CryoSat-2 sea ice draft were calculated. They are listed in table 1 The RMSEs of the data products compared to the mooring data are almost equal and differ in the range of $\pm$ 2 cm. They range from approximately 20-40 cm. The fbRun RMSE is 2.7 cm lower at mooring A, 1.7 cm lower at mooring B and 0.4 cm higher at mooring D than the AWI CryoSat-2 RMSE.

4 Discussion

To show the effect of the assimilation, the RMSE between the assimilated SIC and FB and the modelled SIC and FB was calculated for refRun, sicRun and fbRun. Figure 3 and 4 show that SIC and FB as expected are improved when observations are assimilated. The resulting FB RMSE is well below the observation error used in the Kalman filter (15cm) and the SIC RMSE is slightly higher than the used error of 15 %. This is an artefact resulting from the chosen area over which the RMSEs are calculated and the definition of the RMSE. RMSE weights larger error more than smaller errors. The FB differences are only calculated over an area that is sea ice covered while the SIC data includes large areas, which are seasonal either ice free or ice covered. For SIC, the area with the largest error, which is weighted most, is the ice edge, which increases in space over the winter season. This is what is reflected in the seasonal increase in the SIC RMSE. Other assimilation studies chose to only

https://doi.org/10.5194/tc-2022-262
Preprint. Discussion started: 4 January 2023

The Cryosphere Discussions
Open Access
EGU

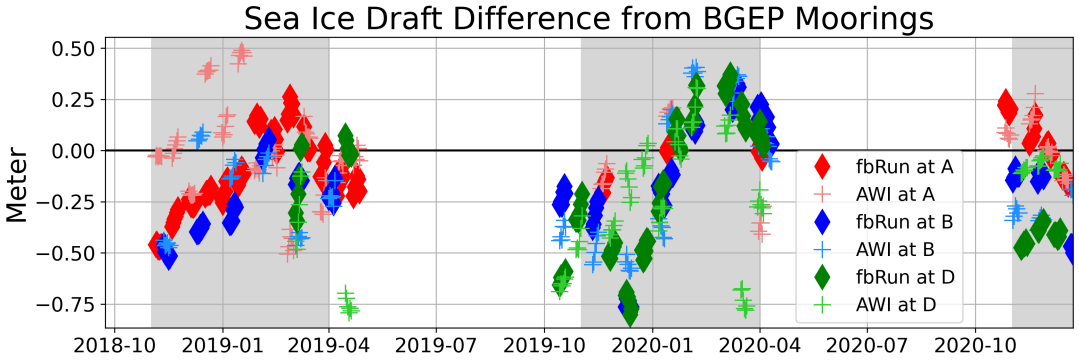

Figure 8. The weekly mean difference between the BGEP upward looking sonar sea ice draft measurements and sea ice draft calculated from the AWI sea ice data set (+) and the fbRun sea ice data (diamonds). The color indicate the location in figure 1. Positive values indicate that the BGEP draft is thicker.

calculate the RMSE over ice areas with SIC > 15 % (Chen et al., 2017). Since the ice edge is the area where the assimilation has the larges effect, we choose to calculate the RMSE over the entire area.

To get a better overview of the development of the RMSE, the assimilated runs are compared to the refRun and the difference between them is plotted in the lower panel of figure 3 and 4. Figure 3 lower panel shows that SIC improves steadily throughout the entire assimilation period for both runs. They both have a similar behaviour, which is expected as they both assimilate the same SIC data.

Figure 4 shows that FB from the fbRun improves the most within approximately the first 5 weeks each year of the assimilation period, whereas FB from the sicRun doesn't improve at all. It is expected that FB from the sicRun does not improve, as it is not assimilated in this run. In the sicRun no sea ice thickness/Snow thickness is added except if the increment suggest ice cover in areas which had prior to the assimilation no ice.

The assimilation of SIC has close to no impact on the FB simulation. At the same time the FB assimilation has, if any, an insignificant impact on the SIC field. This is in good agreement with prior studies investigating the difference between SIC and sea ice thickness assimilation as for example Mu et al. (2018).

The goal of this study is to improve the sea ice thickness estimate by assimilating SIC and FB. To evaluate whether or not the sea ice thickness has improved, the different simulations were compared to BGEP upward looking sonar moorings. Figure 7 shows that the fbRun sea ice draft is closer to the BGEP measurements throughout all seasons and at all three locations, while no improvement is shown for the sicRun. In figure 4 the FB RMSE is still reduced at the onset of the new assimilation season. The improvement of the fbRun sea ice draft shown in figure 7 persists through out the entire 2 year period shown. This suggest that the assimilation of the FB does improve the modelling of the sea ice thickness throughout out the entire summer season and that the fbrun has memory, which last at least a summer season. The first values in each assimilation season in figure 3 and 4 lower panel show which of the two assimilated variables is still improved after the summer season free run. Values below 0 in the lower panel in figure 3 show that the assimilated runs compares worse to the refRun, when they are compared to the

https://doi.org/10.5194/tc-2022-262
Preprint. Discussion started: 4 January 2023

assimilated SIC data. In comparison, the FB values are above 0 cm in all years. Dirkson et al. (2017) and Day et al. (2014) show that SIC has a shorter memory than sea ice thickness. The facts that, FB improves sea ice thickness, as shown in figure 7, and that FB values are continuously improved after the summer season in all years as shown in figure 4 lower panel show that FB also keeps the memory as oppose to SIC.

The BGEP ice draft measurements only cover a very small part of the Arctic Ocean. To get a better Arctic wide evaluation of the effect of the assimilation we also compare the modeled sea ice thickness (from both assimilated and free run) to the AWI data set sea ice thickness. The AWI sea ice thickness has an error of $\pm$ 0.3-0.6 m and is calculated based on the same FB measurements that are used in the assimilation. The data sets are compared in figure 5 for one week in the beginning of the third assimilation period (left panel) and the last week of the same assimilation period (right panel). The distribution of the sea ice thicknesses, shown on the right and upper limits of the plots, show that the fbRun sea ice thickness distribution agrees better with the AWI sea ice thickness distribution compared to the refRun in both weeks. The dominate sea ice thickness values of the refRun and the AWI sea ice thickness agree better with one another than the the fbRun dominate sea ice thickness values, as indicated by the maximum on the outer axis in figure 5. But overall the fbRun sea ice thickness correlate better with the AWI sea ice thickness than the refRun sea ice thickness does. Especially the areas with thick ice has improved when comparing fbRun to the refRun. Over all the AWI sea ice thickness is thicker than both the fbRun and the refRun, especially in areas with thick ice. The biases changes through out the season. In October the AWI sea ice thickness is thicker almost in all locations. In March the refRun and fbRun sea ice thickness is thicker for thin ice. The AWI data set consist of all the variables used in equation 4 to calculate sea ice thickness from FB. To get a better overview over the geographical locations of the difference and the potential origins of the biases in figure 5 the weekly difference maps were plotted for the week following the 30th of March 2020. This is the same data as shown in figure 5 right panel. The first two maps in figure 6 show that the assimilated sea ice thickness is closer to the AWI sea ice thickness than the refRun in most areas just as figure 5. The two right hand panels show the differences between the sea ice density of the AWI data set and the assimilated run and the difference between the snow thickness. Here a clear division in the difference depending on the ice type is visible. The ice type is not shown, but covers the area which is red in the sea ice density difference plot in figure 6 D). Alexandrov et al. (2010) finds that the uncertainties in sea ice density leads to the largest uncertainties in sea ice thickness retrievals in CryoSat-2 products, and Zygmuntowska et al. (2014) finds that the snow uncertainties account most of the sea ice thickness uncertainty. The snow thickness and sea ice density differences in 6 C) and D) show a clear pattern of FYI and MYI, which is not clearly reflected in the thickness difference in 6 B). There could be several reasons for this. The FB in fbRun for example is not exactly the same as the FB used in the AWI sea ice thickness calculation, since it is filtered by PDAF before the increment is calculated. Another reason could be that the higher sea ice density influences the sea ice thickness with the opposite sign compared to the lower snow thickness. Since the FYI area is the area where sea ice density is higher and the snow thickness is lower in figure 6 C) and D) it could be that their effects cancel out. Sievers et. al (in preparation) is a study analysing in more detail what effects the different variables derived from sea ice model have on the calculation of sea ice thickness.

The sea ice thickness uncertainties in the AWI data set, which is displayed in figure 6 range on average from 0.6 m to 1 m. The differences in figure 6 B) are of similar magnitudes. Since the AWI sea ice thickness and the fbRun sea ice thickness differ

https://doi.org/10.5194/tc-2022-262
Preprint. Discussion started: 4 January 2023

on about the same magnitude, as the uncertainties in the AWI sea ice thickness data set both sea ice thicknesses were also compared to the BGEP moorings. The independent sea ice draft measurements of the BGEP moorings are located in the area of the Beaufort sea. In figure 8 the assimilated draft and the AWI data set draft are compared to the three moorings during all time steps in which the three observations coexist in time and space. The calculated RMSE in table 1 shows that the assimilated data is in slightly better agreement with the observations than the AWI data set in two out of three locations. Figure 7 shows that the assimilated sea ice draft is in closer agreement with the BGEP mooring data than the refRun, which is showing better agreement with the AWI sea ice thickness in figure 6 A). This shows that the FB assimilation method presented in this study leads to an improved sea ice thickness estimate both in comparison to the refRun and the AWI sea ice thickness thanks to the use of modeled snow thickness and sea ice density, at least in the Beaufort sea.

5 Conclusions

In this study a method to assimilate FB is described, and the results from a 3 years assimilation run is evaluated. The challenge with assimilation of FB is that it is not a model state variable, but rather a model diagnostic. The presented method builds upon calculating an increment using modeled FB and than converting the changed FB into the sea ice thickness, which is a model state variable. The method uses parameters from the sea ice model for the sea ice density, snow density and snow thickness instead of the prescribed values in the AWI sea ice thickness product. We can show that the assimilation of FB improves both the modeled FB and sea ice thickness.

To compare our method to sea ice thickness data from a more classical approach, we have chosen the weekly sea ice thickness product from the AWI sea ice portal (Hendricks et al., 2021) since it allows a comparison of the two approaches of sea ice thickness calculations based on the same CryoSat-2 FB. Overall the AWI CryoSat-2 sea ice thickness is thicker than the fbRun sea ice thickness. The largest differences might originate from differences in snow thickness and sea ice density which is in good agreement with other studies (Alexandrov et al., 2010; Laxon et al., 2013; Zygmuntowska et al., 2014; Sallila et al., 2019) and one of the prime reasons the presented method was developed. No clear origin for this difference could be found, and more investigation is needed.

When comparing the two sea ice thicknesses to an independent sea ice measurements from the BGEP upward looking sonar data, we can show that our sea ice thickness results are of comparable quality. Evaluating the RMSE of weekly mean differences between the AWI sea ice thickness, fbRun sea ice thickness and the BGEP draft measurements show that they are close to equally well comparing to the measurements. In two of the three locations the fbRun sea ice draft compares slightly better to the BGEP sea ice draft(RMSE are listed in table 1) than the AWI sea ice draft.

5.1 Outlook

It was shown that, the parametrisations of the sea surface density, sea ice density and snow thickness used in the presented method are sufficient to give comparable sea ice thickness as the AWI sea ice thickness product, which follows the conventional method to derive sea ice thickness from CryoSat-2 FB by deriving snow and ice parameters from climatologies, and empirical

https://doi.org/10.5194/tc-2022-262
Preprint. Discussion started: 4 January 2023

values. However, there is room for improvement. For example does CICE v6.3 update included a snow model update which now also includes variable snow density values (Hunke et al., 2021b). Updating CICE to a version after v6.3 could improve the calculation of light velocity correction for the radar FB from model values. Instead of the time dependent parametrisation introduced by Mallett et al. (2020) it would also introduce a spacial varying snow density.

One of the main motivations to assimilate FB instead of sea ice thickness was that FB uncertainty is better known than CryoSat-2 derived sea ice thickness uncertainties. Yet a uniform error was used in this study mainly due for technical reasons. The main aim of this study was to present the method on how to assimilate FB, and as discussed above the presented FB assimilation method gives similar sea ice thickness results as the traditionally derived CryoSat-2 sea ice thickness product it was compared to. Nevertheless, it is recommendable to include the local error estimate included in most radar FB data products in future simulation.

The presented method builds upon modeling the most influential variables of equation 4. These are the snow thickness, the snow density and the sea ice density (Alexandrov et al., 2010). The snow density used in this study does not differ from the snow density used in the AWI data product. The sea surface water density does, but has no significant influence on the sea ice thickness (Alexandrov et al., 2010; Kurtz et al., 2013). The results in figure 8 show that the modeled variables result in comparable results as the empirical values used in the AWI sea ice thickness product. Both the snow thickness and the sea ice density differ and no clear conclusion can be drawn at this point, about which of the parameters are more correct. As the aim of this study was to present the method on how to assimilate FB and a validation of the resulting sea ice thickness, a detailed discussion of the model parameter and the resulting influence on the sea ice thickness when compared to more traditional approaches is not included. This will be the focus of Sievers et al. (in preparation).

Code availability. The code is available upon request, from the contact author.

Author contributions. IS conceived the assimilation set up, implemented it and wrote the manuscript draft. TAR edited and reviewed the manuscript and advised on matter related to the assimilation set up and CICE. LS edited and reviewed the manuscript and advised on CryoSat-2 related matters.

Competing interests. To the knowledge of the authors there are no competing interest

Acknowledgements. The data were collected and made available by the Beaufort Gyre Exploration Program based at the Woods Hole Oceanographic Institution (https://www2.whoi.edu/site/beaufortgyre/) in collaboration with researchers from Fisheries and Oceans Canada at the Institute of Ocean Sciences.

https://doi.org/10.5194/tc-2022-262
Preprint. Discussion started: 4 January 2023

This study is a collaboration between the Danish Meteorological Institute, Aalborg University and the Danish Technical University. It is funded by the Danish State through the National centre for Climate Research.

475 The model input contains Copernicus Climate Change Service information (2021) and neither the European Commission nor ECMWF is responsible for any use that may be made of the Copernicus information or data it contains.

The OSI SAF Sea Ice Index v2.1 is made available athttps://osisaf-hl.met.no/v2p1-sea-ice-index

https://doi.org/10.5194/tc-2022-262
Preprint. Discussion started: 4 January 2023

References

Aaboe, S., Down, E. J., and Eastwood, S.: Product User Manual for the Global sea-ice edge and type Product, Norwegian Meteorological Institute: Oslo, Norway, 2021.

Alexandrov, V., Sandven, S., Wahlin, J., and Johannessen, O.: The relation between sea ice thickness and freeboard in the Arctic, The Cryosphere, 4, 373–380, 2010.

Blockley, E. W., Martin, M. J., McLaren, A. J., Ryan, A. G., Waters, J., Lea, D. J., Mirouze, I., Peterson, K. A., Sellar, A., and Storkey, D.: Recent development of the Met Office operational ocean forecasting system: an overview and assessment of the new Global FOAM forecasts, Geoscientific Model Development, 7, 2613–2638, https://doi.org/10.5194/gmd-7-2613-2014, 2014.

Cao, Y., Liang, S., Sun, L., Liu, J., Cheng, X., Wang, D., Chen, Y., Yu, M., and Feng, K.: Trans-Arctic shipping routes expanding faster than the model projections, Global Environmental Change, 73, 102 488, 2022.

Chen, Z., Liu, J., Song, M., Yang, Q., and Xu, S.: Impacts of assimilating satellite sea ice concentration and thickness on Arctic sea ice prediction in the NCEP Climate Forecast System, Journal of Climate, 30, 8429–8446, 2017.

Cox, G. F. and Weeks, W. F.: Salinity variations in sea ice, Journal of Glaciology, 13, 109–120, 1974.

Dai, A. and Trenberth, K. E.: Estimates of freshwater discharge from continents: Latitudinal and seasonal variations, Journal of hydrometeorology, 3, 660–687, 2002.

Day, J., Hawkins, E., and Tietsche, S.: Will Arctic sea ice thickness initialization improve seasonal forecast skill?, Geophysical Research Letters, 41, 7566–7575, 2014.

Dirkson, A., Merryfield, W. J., and Monahan, A.: Impacts of sea ice thickness initialization on seasonal Arctic sea ice predictions, Journal of Climate, 30, 1001–1017, 2017.

Drinkwater, M. R., Francis, R., Ratier, G., and Wingham, D. J.: The European Space Agency's earth explorer mission CryoSat: measuring variability in the cryosphere, Annals of Glaciology, 39, 313–320, 2004.

Egbert, G. D. and Erofeeva, S. Y.: Efficient inverse modeling of barotropic ocean tides, Journal of Atmospheric and Oceanic technology, 19, 183–204, 2002.

Fetterer, F. and Stewart, J. S.: U.S. National Ice Center Arctic and Antarctic Sea Ice Concentration and Climatologies in Gridded Format, Version 1, https://doi.org/10.7265/46cc-3952, 2020.

Fiedler, E. K., Martin, M. J., Blockley, E., Mignac, D., Fournier, N., Ridout, A., Shepherd, A., and Tilling, R.: Assimilation of sea ice thickness derived from CryoSat-2 along-track freeboard measurements into the Met Office's Forecast Ocean Assimilation Model (FOAM), The Cryosphere, 16, 61–85, 2022.

Garnier, F., Fleury, S., Garric, G., Bouffard, J., Tsamados, M., Laforge, A., Bocquet, M., Fredensborg Hansen, R. M., and Remy, F.: Advances in altimetric snow depth estimates using bi-frequency SARAL and CryoSat-2 Ka–Ku measurements, The Cryosphere, 15, 5483–5512, 2021.

Hendricks, S., Ricker, R., and Paul, S.: Product User Guide & Algorithm Specification: AWI CryoSat-2 Sea Ice Thickness (version 2.4), 2021.

Hersbach, H., Bell, B., Berrisford, P., Hirahara, S., Horányi, A., Muñoz Sabater, J., Nicolas, J., Peubey, C., Radu, R., Schepers, D., Simmons, A., Soci, C., Abdalla, S., Abellan, X., Balsamo, G., Bechtold, P., Biavati, G., Bidlot, J., Bonavita, M., De Chiara, G., Dahlgren, P., Dee, D., Diamantakis, M., Dragani, R., Flemming, J., Forbes, R., Fuentes, M., Geer, A., Haimberger, L., Healy, S., Hogan, R. J., Hólm, E., Janisková, M., Keeley, S., Laloyaux, P., Lopez, P., Lupu, C., Radnoti, G., de Rosnay, P., Rozum, I., Vamborg, F., Villaume, S., and Thépaut,

https://doi.org/10.5194/tc-2022-262
Preprint. Discussion started: 4 January 2023

J.-N.: Complete ERA5: Fifth generation of ECMWF atmospheric reanalyses of the global climate, Copernicus Climate Change Service (C3S) Data Store (CDS), accessed in 2021, 2017.

Hordoir, R., Skagseth, Ø., Ingvaldsen, R. B., Sandø, A. B., Löptien, U., Dietze, H., Gierisch, A. M., Assmann, K. M., Lundesgaard, Ø., and Lind, S.: Changes in Arctic Stratification and Mixed Layer Depth Cycle: A Modeling Analysis, Journal of Geophysical Research: Oceans, 127, e2021JC017 270, 2022.

Hunke, E., Lipscomb, W., Jones, P., Turner, A., Jeffery, N., and Elliott, S.: CICE, The Los Alamos sea ice model, Tech. rep., Los Alamos National Lab.(LANL), Los Alamos, NM (United States), 2017.

Hunke, E., Allard, R., Bailey, D. A., Blain, P., Craig, A., Dupont, F., DuVivier, A., Grumbine, R., Hebert, D., Holland, M., Jeffery, N., Lemieux, J.-F., Osinski, R., Rasmussen, T., Ribergaard, M., Roberts, A., Turner, M., Winton, M., and Rethmeier, S.: CICE Version 6.2.0, https://github.com/CICE-Consortium/CICE/tree/CICE6.2.0, 2021a.

Hunke, E., Allard, R., Bailey, D. A., Blain, P., Craig, A., Dupont, F., DuVivier, A., Grumbine, R., Hebert, D., Holland, M., Jeffery, N., Lemieux, J.-F., Osinski, R., Rasmussen, T., Ribergaard, M., Roberts, A., Turner, M., Winton, M., and Rethmeier, S.: CICE Version 6.3.0, https://github.com/CICE-Consortium/CICE/tree/CICE6.3.0, 2021b.

Ivanova, N., Johannessen, O. M., Pedersen, L. T., and Tonboe, R. T.: Retrieval of Arctic Sea Ice Parameters by Satellite Passive Microwave Sensors: A Comparison of Eleven Sea Ice Concentration Algorithms, IEEE Transactions on Geoscience and Remote Sensing, 52, 7233–7246, https://doi.org/10.1109/TGRS.2014.2310136, 2014.

Kaminski, T., Kauker, F., Toudal Pedersen, L., Voßbeck, M., Haak, H., Niederdrenk, L., Hendricks, S., Ricker, R., Karcher, M., Eicken, H., et al.: Arctic mission benefit analysis: impact of sea ice thickness, freeboard, and snow depth products on sea ice forecast performance, The Cryosphere, 12, 2569–2594, 2018.

Kern, S., Khvorostovsky, K., Skourup, H., Rinne, E., Parsakhoo, Z., Djepa, V., Wadhams, P., and Sandven, S.: The impact of snow depth, snow density and ice density on sea ice thickness retrieval from satellite radar altimetry: results from the ESA-CCI Sea Ice ECV Project Round Robin Exercise, The Cryosphere, 9, 37–52, 2015.

Kurtz, N., Farrell, S., Studinger, M., Galin, N., Harbeck, J., Lindsay, R., Onana, V., Panzer, B., and Sonntag, J.: Sea ice thickness, freeboard, and snow depth products from Operation IceBridge airborne data, The Cryosphere, 7, 1035–1056, 2013.

Kurtz, N. T. and Farrell, S. L.: Large-scale surveys of snow depth on Arctic sea ice from Operation IceBridge, Geophysical Research Letters, 38, 2011.

Kwok, R.: Satellite remote sensing of sea-ice thickness and kinematics: a review, Journal of Glaciology, 56, 1129–1140, 2010.

Kwok, R. and Cunningham, G.: Variability of Arctic sea ice thickness and volume from CryoSat-2, Philosophical Transactions of the Royal Society A: Mathematical, Physical and Engineering Sciences, 373, 20140 157, 2015.

Kwok, R., Panzer, B., Leuschen, C., Pang, S., Markus, T., Holt, B., and Gogineni, S.: Airborne surveys of snow depth over Arctic sea ice, Journal of Geophysical Research: Oceans, 116, 2011.

Laxon, S., Peacock, N., and Smith, D.: High interannual variability of sea ice thickness in the Arctic region, Nature, 425, 947–950, 2003.

Laxon, S. W., Giles, K. A., Ridout, A. L., Wingham, D. J., Willatt, R., Cullen, R., Kwok, R., Schweiger, A., Zhang, J., Haas, C., et al.: CryoSat-2 estimates of Arctic sea ice thickness and volume, Geophysical Research Letters, 40, 732–737, 2013.

Lellouche, J.-M., Greiner, E., Bourdallé-Badie, R., Garric, G., Melet, A., Drévillon, M., Bricaud, C., Hamon, M., Le Galloudec, O., Regnier, C., et al.: The Copernicus global 1/12° oceanic and sea ice GLORYS12 reanalysis, Frontiers in Earth Science, 9, 585, 2021.

Madec, G., Bourdallé-Badie, R., Bouttier, P.-A., Bricaud, C., Bruciaferri, D., Calvert, D., Chanut, J., Clementi, E., Coward, A., Delrosso, D., et al.: NEMO ocean engine, 2017.

https://doi.org/10.5194/tc-2022-262
Preprint. Discussion started: 4 January 2023

Mallett, R. D., Lawrence, I. R., Stroeve, J. C., Landy, J. C., and Tsamados, M.: Brief communication: Conventional assumptions involving the speed of radar waves in snow introduce systematic underestimates to sea ice thickness and seasonal growth rate estimates, The Cryosphere, 14, 251–260, 2020.

Martino, A. J., Neumann, T. A., Kurtz, N. T., and McLennan, D.: ICESat-2 mission overview and early performance, in: Sensors, systems, and next-generation satellites XXIII, vol. 11151, pp. 68–77, SPIE, 2019.

Mu, L., Yang, Q., Losch, M., Losa, S. N., Ricker, R., Nerger, L., and Liang, X.: Improving sea ice thickness estimates by assimilating CryoSat-2 and SMOS sea ice thickness data simultaneously, Quarterly Journal of the Royal Meteorological Society, 144, 529–538, 2018.

Nerger, L., Janjić, T., Schröter, J., and Hiller, W.: A regulated localization scheme for ensemble-based Kalman filters, Quarterly Journal of the Royal Meteorological Society, 138, 802–812, 2012.

OSISAF: Global Sea Ice Concentration Climate Data Record v2. 0–Multimission, EUMETSAT SAF on Ocean and Sea Ice, 2017.

Ricker, R., Hendricks, S., Helm, V., Skourup, H., and Davidson, M.: Sensitivity of CryoSat-2 Arctic sea-ice freeboard and thickness on radar-waveform interpretation, The Cryosphere, 8, 1607–1622, 2014.

Sallila, H., Farrell, S. L., McCurry, J., and Rinne, E.: Assessment of contemporary satellite sea ice thickness products for Arctic sea ice, The Cryosphere, 13, 1187–1213, 2019.

Schulzweida, U.: CDO User Guide, https://doi.org/10.5281/zenodo.7112925, 2022.

Smith, G. C., Liu, Y., Benkiran, M., Chikhar, K., Surcel Colan, D., Gauthier, A.-A., Testut, C.-E., Dupont, F., Lei, J., Roy, F., et al.: The Regional Ice Ocean Prediction System v2: a pan-Canadian ocean analysis system using an online tidal harmonic analysis, Geoscientific Model Development, 14, 1445–1467, 2021.

Stroeve, J. and Notz, D.: Insights on past and future sea-ice evolution from combining observations and models, Global and Planetary Change, 135, 119–132, 2015.

Tilling, R. L., Ridout, A., and Shepherd, A.: Estimating Arctic sea ice thickness and volume using CryoSat-2 radar altimeter data, Advances in Space Research, 62, 1203–1225, 2018.

Timco, G. and Frederking, R.: A review of sea ice density, Cold regions science and technology, 24, 1–6, 1996.

Tsamados, M., Feltham, D. L., Schroeder, D., Flocco, D., Farrell, S. L., Kurtz, N., Laxon, S. W., and Bacon, S.: Impact of variable atmospheric and oceanic form drag on simulations of Arctic sea ice, Journal of Physical Oceanography, 44, 1329–1353, 2014.

Vernieres, G., Zhao, B., Cullather, R. I., Akella, S., Vikhliaev, Y. V., Kurtz, N. T., and Kovach, R. M.: Assimilation of Cryosat 2 Arctic Sea-Ice Freeboard in an Ensemble of Coupled GEOS5, American Geophysical Union, 2016, HE13A–06, 2016.

Warren, S. G., Rigor, I. G., Untersteiner, N., Radionov, V. F., Bryazgin, N. N., Aleksandrov, Y. I., and Colony, R.: Snow depth on Arctic sea ice, Journal of Climate, 12, 1814–1829, 1999.

Zygmuntowska, M., Rampal, P., Ivanova, N., and Smedsrud, L. H.: Uncertainties in Arctic sea ice thickness and volume: new estimates and implications for trends, The Cryosphere, 8, 705–720, 2014.